Geminate Rebinding and Conformational Dynamics of Myoglobin Embedded in a Glass at Room Temperature

Stephen J. Hagen, James Hofrichter, and William A. Eaton*

Laboratory of Chemical Physics, Building 5, National Institutes of Health, Bethesda, Maryland 20892-0520

Received: January 23, 1996; In Final Form: May 17, 1996[⊗]

Below the glycerol/water glass transition (∼180 K), myoglobin exhibits distributed geminate rebinding kinetics as a result of "frozen" conformational substates (Austin et al. *Biochemistry* **1975**, *14*, 5355). As the temperature is increased through the solvent glass transition, the apparent rate of geminate rebinding *decreases*. This slowing has been attributed to a protein relaxation that impedes CO rebinding at high *T*, but that is itself prevented at low *T* by energetic barriers to conformational change (Steinbach et al. *Biochemistry* **1991**, *30*, 3988). Using time-resolved spectroscopy with nanosecond lasers, we have studied ligand rebinding in sperm whale MbCO embedded in a glass at room temperature. Over a wide temperature range $T = 105-297$ K, the kinetics of rebinding are well characterized by the same inhomogeneous distribution $g(H_{BA})$ of enthalpy barriers H_{BA}, and changes in the shape of the Soret difference spectrum during rebinding can be explained by "kinetic hole burning". That is, at sufficiently high viscosity the multiexponential "low temperature" rebinding of MbCO can be observed at all *T*, as predicted by Ansari et al. (*Science* **1992**, *256*, 1796). Moreover, the average geminate rate predicted from the observed rate distribution is ∼2500 times larger than the geminate rate in the completely relaxed protein in aqueous solution (Ansari et al. *Biochemistry* **1994**, *33*, 5128). Thus, we have shown that high solvent viscosity prevents both interconversion of conformational substates and functionally important relaxation in the interior of the protein, independent of *T*.

Introduction

Beginning with the pioneering time-resolved spectroscopic and kinetic studies of Hochstrasser,[1] Frauenfelder,[2] and their co-workers in the 1970s, flash photolysis studies of heme proteins have provided an increasingly detailed picture of the complex interactions between proteins and their ligands. These studies have shown that structural inhomogeneity, fluctuations, and conformational changes of the protein have important effects on both the reaction at the heme and the transport of ligands through the protein molecule. The kinetics of transitions between conformational substates and changes in average structure are controlled by both protein energy barriers and solvent viscosity. In this work we demonstrate that, over a wide range of temperature, solvent viscosity can be the important factor in determining the rates of conformational changes. We find that sufficiently high solvent viscosity can almost completely suppress both transitions between conformational substates and the change in average conformation that follows photodissociation of the heme−ligand complex in myoglobin.

Experiments on the photodissociation of the heme−CO complex in MbCO show that, at temperatures below the glass transition temperature of the solvent ($T_g \sim 180$ K for 75%/25% v:v glycerol/water mixtures), each Mb molecule is trapped within one of many similar, but kinetically distinct, low-energy structures or substates.[2,3] Because each substate exhibits a different rate for the geminate rebinding of the photodissociated CO ligand, the rebinding of a population of molecules resembles a superposition of exponential processes with different rates. At room temperature, the rebinding kinetics become more nearly exponential, indicating that a single average rate characterizes the rebinding of all molecules. The energy barriers separating protein substates are therefore sufficiently small to allow rapid thermal averaging at room *T*, with each molecule sampling many substates on the nanosecond time scale of ligand rebinding.[4]

The rebinding kinetics at temperatures near the solvent glass transition are more complicated. Curiously, the average rate of geminate rebinding decreases as *T* increases through T_g.[2,3] This slowing was initially interpreted as arising from the escape of the ligand to outer wells in the protein.[2,5] More recently it has been attributed to an increase in the activation energy *H* for geminate recombination of the ligand.[3,6] This increase was in turn attributed to a global structural relaxation of the protein, not yet time-resolved, observed by X-ray crystallography and initiated by a displacement of the iron atom away from the mean porphyrin plane upon ligand dissociation.[7] At temperatures below T_g, the relaxation is presumed to be "frozen out" by energy barriers that separate conformational states of the protein.[3,6] Because the inhomogeneous kinetics at low temperature (i.e., the absence of thermal averaging over substates with different geminate rates) were also attributed to these energy barriers, the "landscape" of energies associated with the many possible protein conformations controls the conformational kinetics of myoglobin.[8]

Recent experiments[4,9−11] have shown that photodissociation of MbCO in aqueous solvent near 300 K initiates a rapid conformational change in the protein. The relaxation can be time-resolved as a shift in both the Soret band[4,9,10] and the near-infrared (760 nm) band[11] of Mb after photodissociation of the ligand. Anfinrud and co-workers[11] showed that this relaxation is highly nonexponential, extending from less than 2 ps to nearly 1 μs after photolysis. Ansari et al.[9,12] studied the effect of solvent viscosity on the latter portion of this relaxation for $\eta \approx 1-300$ cP, $T = 268-308$ K. Their modeling of both the ligand rebinding and spectral kinetics indicated that this relaxation could indeed increase the activation energy for ligand rebinding, with the result that it slows the rate of geminate rebinding by at least a factor ∼100 at room temperature. They also found

[⊗] Abstract published in *Advance ACS Abstracts,* July 1, 1996.

S0022-3654(96)00219-5

that the rate of protein conformational relaxation κ^* slows significantly as solvent viscosity increases at fixed T. In fact, κ^* exhibits the behavior of a Kramers-like unimolecular reaction rate in the presence of high friction:[13]

$$\kappa^*(T,\eta) \approx [C/(\sigma + \eta)] \exp(-E_0/RT) \qquad (1)$$

where $C \approx 7.2 \times 10^{10}$ cP/s, $R = 8.31$ J/(mol·K), and $E_0 \approx 10$ kJ/mol describes the energy barrier for relaxation.[9,12] E_0 includes the energy of interaction between the protein and the solvent, averaged over an equilibrium distribution of solvent coordinates. The parameter $\sigma \approx 4$ cP was introduced to represent the contribution of the protein internal friction towards the total reaction friction. In eq 1 two factors separately control the rate of conformational relaxation: the energy barriers associated with conformational changes control the Arrhenius-like exponential term $\exp(-E_0/RT)$, and the solvent viscosity contributes to the prefactor $1/(\sigma + \eta)$. Because of the small value $\sigma \approx 4$ cP obtained for the internal protein friction, i.e., comparable to the room T viscosity of water ($\approx$1 cP), κ^* is sensitive to changes in solvent viscosity. Ansari et al. observed that eq 1, obtained at high temperature, could have important consequences for the low-temperature conformational kinetics of myoglobin. The slow kinetics at low T were originally attributed to the energy landscape of the protein, but if the solvent undergoes a glass transition,[14] for which $\eta \rightarrow 10^{15}$ cP, eq 1 implies an overwhelming suppression of the relaxation rate κ^* by the viscosity-dependent prefactor as $T \rightarrow T_g$. In this case protein relaxation would slow dramatically as T decreases, not because of the diminishing size of RT relative to the energy barrier E_0, but because exponential growth[15] of solvent viscosity near T_g imposes enormous friction on barrier crossings, resulting in slow dynamics.

Thus, the well-documented slowing of conformational dynamics in myoglobin in glycerol/water solutions below 200 K may result primarily from the rapidly increasing solvent viscosity near T_g, rather than from energy barriers associated with conformational changes in the protein. This has been called a "slaved glass" transition by Frauenfelder and co-workers,[16,17] and has been observed in the kinetics of conformer equilibration in liganded myoglobin following a pressure change.[16] Ansari et al.[9,12] suggested that, if solvent friction is the primary influence on dynamics, a sufficiently viscous solvent might suppress both relaxation and interconversion between conformational states of Mb even at high temperatures. Inhomogeneous, nonexponential geminate kinetics, like those observed below 200 K, would then be observed in Mb at room temperature.

An early study of solvent viscosity and ligand binding kinetics in myoglobin presented a different picture. Beece et al.[5] studied the motion of small ligands through myoglobin in the context of a sequential model, in which the ligand moves through a (nonrelaxing) protein by passing through a series of states separated by enthalpy barriers. They found that, at low viscosity, the transition between two states $i \rightarrow j$ could be modeled with a rate

$$k_{ij}(\eta,T) = (A_{ij}^{\ 0} + A_{ij}/\eta^{\kappa}) \exp(-H_{ij}/RT) \qquad (2)$$

Like eq 1, this relation was based on Kramers' theory for the friction dependence of a unimolecular rate, but eq 2 includes the additive constant $A_{ij}^{\ 0}$ and the more complicated viscosity dependence. Beece et al. modified Kramers' rate on the grounds that ligand motion through the protein requires internal protein motions that are hindered but never entirely prevented by high solvent viscosity. Thus, even in the event of a solvent glass transition, the ligand still moves through the protein. However, these authors did not consider a link between protein relaxation and geminate rebinding and therefore did not directly consider the potential effect of viscosity on that relaxation. That question was considered by Steinbach et al.,[3] who reanalyzed the data of Beece et al. and concluded that solvent viscosity has little or no effect on conformational relaxation in Mb. Frauenfelder et al.[18] later reevaluated the evidence and argued that solvent viscosity does control the rate of relaxation through a Kramers-like relationship $\kappa^*(T) \propto \eta^{-\mu}$ (where $0 < \mu < 1$). Recently, however, Nienhaus et al.[19] proposed that the absorption of light can induce conformational relaxation in Mb at low T, even when the protein is embedded in a solid environment. This would suggest that high solvent viscosity alone cannot prevent conformational relaxation.

The only other available data on myoglobin ligand binding kinetics under conditions of high viscosity is that of Austin et al.,[2] who studied ligand recombination in myoglobin dried in poly(vinyl alcohol) at room temperature. These authors observed distributed geminate rebinding rates under these conditions, but the kinetics were complex, with several additional unexplained processes apparent above 200 K. These may have been due to protein relaxation. However, these authors' single-wavelength measurements provided no information about conformational relaxation occuring during rebinding.

In analyzing the effects of viscosity, we have discussed conformational relaxation and interconversion of conformational substates separately, even though Ansari et al.[9,12] proposed that viscosity would affect both processes similarly. This separate treatment is for reasons that are in part historical. Conformational relaxation kinetics have been directly studied only near room temperature, where it has been assumed that thermal averaging of the substates is fast compared to relaxation.[12,20] An opposite (and unphysical) assumption has also been made: Steinbach et al.[3] suggested that conformational relaxation can occur without any interconversion of conformational substates. Hagen and Eaton have recently proposed a model that clarifies the relation between interconversion of conformational substates and conformational relaxation.[21] They show that the observed nonexponential conformational relaxation in fact indicates that substates are interconverting, but that thermal averaging is incomplete. In the Hagen/Eaton model, the conformational relaxation that follows photodissociation is the redistribution of the population of protein molecules from one set of substates to another. Prior to photolysis, the molecules occupy a group of substates that represent the low-energy conformations available to the liganded molecule. After photolysis, transitions take place from these states to a new group of states at lower energy, representing the energetically favorable conformations of the unliganded molecule. If the transition states for all transitions between substates share a common energy $E^{\dagger}$, the activation energy for a transition from a substate at energy E_i to any other substate is simply $E^{\dagger} - E_i$. This activation energy causes exponential slowing of the conformational kinetics as the average conformational energy of the molecules decreases. The dramatic slowing of the rate of conformational change as the system approaches equilibrium readily accounts for the highly "stretched" ($\beta \sim 0.1$ in $\exp[-(\kappa^* t)^{\beta}]$) exponential time course observed by Anfinrud and co-workers.[11] The importance of the Hagen/Eaton model for the present study is that it identifies substate interconversion and conformational relaxation as a single process. Suppression of transitions between conformational substates immediately implies suppression of conformational relaxation and vice versa. Agmon et al.'s recent study of Mb ligand binding kinetics in glycerol/water solvent supports

this picture, since it indicates that, as temperature increases, the onset of protein conformational relaxation coincides with the onset of substate interconversion.[22]

In order to test the prediction of Ansari et al.[9,12] that both types of conformational change can be suppressed by high solvent viscosity, we have studied ligand binding in MbCO embedded in a glass at room temperature. We placed sperm whale myoglobin in a solution of water and trehalose, which undergoes a glass transition upon dehydration at room temperature.[23] This transition locks the protein into a rigid solid with viscosity[14] $\eta > 10^{15}$ cP; the MbCO complex can be photodissociated under these conditions by a nanosecond laser pulse, and the geminate recombination of the ligand can then be observed over a wide temperature range $T \approx 100-300$ K by time-resolved absorption spectroscopy in the Soret spectral region. By studying spectral changes associated with ligand recombination, we have found that the glassy environment suppresses conformational relaxation and interconversion of protein substates at all temperatures $T \leq 300$ K. We also find that the unrelaxed conformations of the protein that are trapped by the glassy solvent exhibit a significantly higher rate of geminate rebinding than is observed in the relaxed protein after photodissociation in aqueous solvents; this may offer the most direct evidence that conformational relaxation of myoglobin slows the rate of ligand binding. The data analysis is complicated by the intrinsic temperature dependence of both the liganded and unliganded spectra. We have overcome this problem through an elaborate (although necessary) procedure that separates these spectral effects from the kinetic analysis. A brief report of this work has appeared elsewhere.[24]

The glass-forming agent, trehalose, is a disaccharide that is strongly associated with the biological phenomenon of anhydrobiosis. This is the ability of some organisms (e.g., baker's yeast, brine shrimp) to survive extended periods of dehydration.[25] Trehalose is found in high concentration in the cells of many of these organisms, and although the mechanism of its action remains under study,[23,25] Green and Angell have suggested that the glass transition in trehalose serves to protect membranes and proteins from damage or denaturation under dry conditions. Codrying with trehalose has been shown *in vitro* to enhance profoundly the ability of delicate enzymes to withstand dehydration and elevated temperature without loss of structure or activity.[25,26] A trehalose glass is therefore presumed to have no deleterious interaction with the protein. Trehalose glass has recently been used to capture photointermediates of rhodopsin at room temperature.[27] Finally, we note that the unique properties of trehalose may make it very suitable as a storage medium for hemoglobin based blood substitutes.[28]

Materials and Experimental Procedure

Samples of carbonmonoxymyoglobin embedded in trehalose glass were prepared by dehydration of a concentrated myoglobin/buffer/trehalose solution at room temperature under a carbon monoxide (CO) atmosphere. Lyophilized sperm whale skeletal muscle metmyoglobin (Sigma M-0380) was purified by gel filtration on Sephacryl S-100HR at pH 8.0 in 20 mM Tris-HCl buffer, then concentrated by N_2-pressure ultrafiltration and centrifugal concentration to [Mb] $\approx$ 0.7 mM. This protein solution was then degassed by stirring under water-saturated Ar, and 0.6 g/mL of crystalline trehalose dihydrate (Sigma T-9531) was dissolved into the Mb solution. The metmyoglobin was subsequently reduced by the addition of sodium dithionite and equilibrated with 1 atm of CO.

Individual dehydrated samples were prepared by spreading the myoglobin/trehalose solution in a uniform thin layer ($\sim$0.5 $\times$ 1.0 cm^2) on a microscope slide. The applied volume was chosen so as to yield a layer with an optical density of 0.6−0.8 at the MbCO Soret absorption peak. Under flowing dry CO, the MbCO/trehalose mixture quickly forms a transparent film adhering to the slide: after 1−2 days of further drying the film hardens to a clear glass ($\sim$20−50 μm thick) with a total water content estimated (by weighing) at $\sim$3.5 wt% indicating a glass transition temperature[23] $T_g \approx 40-50$ °C. The sample was then coated with a protective layer of optical-grade epoxy and sealed with a glass cover slip. This coating limits thermal-expansion damage to the trehalose film and slows any loss of CO to the vacuum environment of the spectrometer dewar.

The sample slide was cemented to a copper stage between the quartz windows of a liquid nitrogen optical dewar. The sample temperature was detected by a silicon diode sensor and regulated by resistive heaters in a conventional cryogenic temperature control circuit. A fine-gauge chromel−constantan thermocouple (125 μm diameter) was attached to the sample to verify that significant temperature gradients did not develop between the sample and the sensor diode.

Time-resolved optical absorption in the Soret region of the Mb spectrum was measured with a transient spectrometer[29] employing the 10 ns pulses of two Nd:YAG lasers. The 1064 nm fundamental of the first laser is frequency-doubled to generate a photolysis pulse at 532 nm, while the 355 nm third harmonic of the second laser excites the fluorescence of stilbene dye to produce a broad-wavelength probe pulse. A 1/4-m spectrograph projects the probe light spectrum from both photolyzed and reference regions of the sample onto a silicon vidicon detector. By varying the delay time between the photolysis and probe pulses, we obtained the time-resolved spectra of the photolyzed sample on a combined linear and logarithmic time scale, from $\approx$−20 ns (prior to peak photolysis) up to a maximum delay greater than 0.1 s. We collected data at temperature intervals of 10−20 K between room temperature and $\approx$100 K. Below 100 K the recovery of the photolyzed sample becomes too slow for practical data collection with the present detection and timing system.

Absorption data collected at each temperature were converted to a set of difference optical spectra (i.e., photolyzed−unphotolyzed sample spectra) and form matrices $\mathbf{a}(\lambda,t,T)$ in measured wavelengths λ (=396−470 nm) and delay times t. These data matrices were analyzed by singular value decomposition[30] (SVD), in which the matrix $\mathbf{a}(\lambda,t,T)$ is reconstructed as the product of three component matrices $\mathbf{a}(\lambda,t,T) = \mathbf{v}(t,T)\,\mathbf{s}(T)\,\mathbf{u}(\lambda,T)^{\mathrm{T}}$. The columns of $\mathbf{u}(\lambda,T)$ describe a set of orthonormal component spectra $u_i(\lambda,T)$ from which the data can be reconstructed, while the columns of $\mathbf{v}(t,T)$ contain the (normalized) time dependence $v_i(t,T)$ associated with each component spectrum i. The singular values $s_i(T)$, or elements of the diagonal matrix $\mathbf{s}(T)$, fix the relative sizes of the contributions made by the component spectra and are sorted in order of decreasing size. In the SVD treatment, the first n elements of **s** and the first n columns of the matrices **u** and **v** together provide the best n-component least-squares representation of the data matrix **a**. Only the first 12 SVD components of each data set were retained, sharply reducing the size of the data set while preserving all significant spectral and kinetic information. A rotation procedure[30] was then applied to the reduced data set in order to remove most time-dependent random noise from the lower-order components of $\mathbf{v}(t,T)$.

Results

Time-resolved photolysis difference spectra were recorded at 14 temperatures T from 105 to 297 K. In our initial analysis,

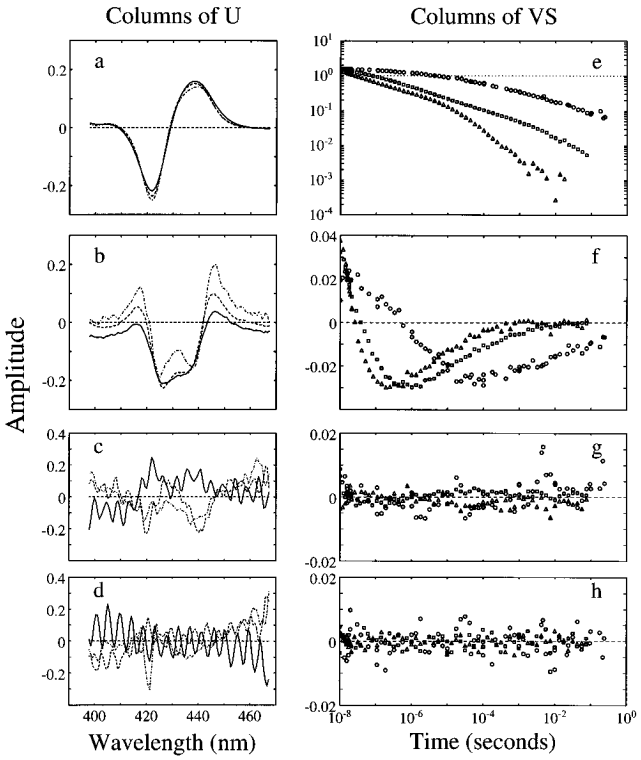

Figure 1. (a−d) The four most significant spectral components $u_1(\lambda,T)$ − $u_4(\lambda,T)$ from individual data sets collected at $T = 275$ K (solid line), 208 K (broken line), and 105 K (dot-dash line), after removal of offsets. (e−h) The associated amplitudes $v_1(t)s_1 - v_4(t)s_4$ at $T = 275$ K (up triangle), 208 K (open box), and 105 K (open circle).

each set of spectra (corresponding to one temperature) was analyzed individually by singular value decomposition (SVD). The data from all temperatures were then analyzed together by global SVD and corrected for the effects of the temperature dependence of the Mb Soret spectra. We first summarize the principal results of the initial data analysis, and we present two arguments that support the conclusion that the observed changes in the shape of the photoproduct spectra with time originate from the more rapid rebinding of CO to those portions of the photoproduct population that exhibit red-shifted deoxy and CO spectra. This phenomenon, known as kinetic hole burning, was first observed in Mb at low temperature by Friedman and coworkers.[31,32] We then describe the procedure by which the data were globally analyzed and the temperature corrections made. Finally, we describe how the corrected data were successfully fitted to a kinetic hole burning model in which no conformational relaxation occurs prior to ligand rebinding.

Initial Analysis. Figure 1 shows the largest SVD components and amplitudes for three representative data sets, collected at $T = 275$, 208, and 105 K. The first two or three SVD components at each temperature contain essentially all the kinetic and spectral information. The first component $u_1(\lambda,T)$ represents an average Mb−MbCO Soret difference spectrum at T; the associated amplitude $v_1(t,T)$ is proportional to the fraction $N(t,T)$ of photolyzed hemes remaining unliganded a time t after the photolysis laser pulse. The second component $u_2(\lambda,T)$, whose singular value $s_2(T)$ is 2−2.5% as large as $s_1(T)$, forms the leading correction to the average difference spectrum. $u_2(\lambda,T)$ is similar at all temperatures and resembles a sum of the derivatives (with respect to wavelength) of the Mb and MbCO Soret peaks. This component therefore describes a wavelength shift of the Mb and MbCO Soret spectra, and its time dependence $v_2(t,T)$ indicates that both spectra shift to shorter wavelength during rebinding. The third component

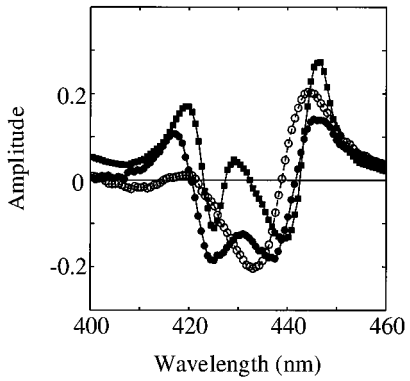

Figure 2. $U_2(\lambda)$ for MbCO in glycerol/buffer at $T = 300$ K (open circle), 190 K (solid circle), and difference of normalized successive difference spectra Mb−MbCO in glycerol/buffer at $T = 40$ K (solid box), from Ormos et al.[33]

$u_3(\lambda,T)$ describes an additional, much smaller correction ($s_3(T)/s_1(T) \leq 0.3\%$), but the generally poor signal-to-noise ratio of this component does not allow a meaningful interpretation of its origin.

A qualitative examination of the spectral changes that accompany ligand rebinding in trehalose provides the first evidence that these changes arise from kinetic hole burning at all temperatures. We utilize the well-characterized behavior of Mb in glycerol/buffer[31,33] as a point of reference. In Figure 2 we illustrate the qualitatively different spectral changes that can be attributed to hole burning *vs.* relaxation. Figure 2 shows the second SVD components $u_2(\lambda,T)$ of the photolysis difference spectra of sperm whale myoglobin in glycerol/buffer at $T = 300$ K and $T = 190$ K. Figure 2 also shows an analogous measurement at very low temperature, the normalized difference between successive time-resolved difference spectra for MbCO in glycerol/buffer at $T = 40$ K, from Figure 5 of Ormos et al.[33] The spectral changes occuring in photolyzed MbCO at $T \leq 60$ K have been shown to result exclusively from kinetic hole burning rather than structural relaxation,[31] while at $T \approx 300$ K significant heme relaxation is known to occur after photolysis.[9,12] The shape of $u_2(\lambda,T)$ at 190 K in Figure 2 therefore provides a spectral signature of hole burning in the Mb−MbCO Soret region, while that at 300 K characterizes the spectral changes resulting from relaxation of the deoxy photoproduct prior to ligand rebinding. Over the entire temperature range studied, $u_2(\lambda,T)$ for MbCO in trehalose (Figure 1b) is much more similar to the hole burning spectrum (Figure 2, 190 K, 40 K) than the relaxation spectrum (Figure 2, 300 K). This similarity provides strong evidence that the spectral changes coincident with ligand rebinding are primarily due to hole burning.

Quantitative evidence that the second SVD component describes hole burning rather than protein relaxation is obtained from a straightforward analysis of the time dependence of $N(t,T)$ and the average wavelength $\langle\lambda\rangle$ of the photoproduct spectrum. Agmon[34] has noted that the absorption spectrum of an inhomogeneously broadened rebinding system will show a "universal" behavior: the position of the center wavelength $\langle\lambda\rangle$ during rebinding is a function only of the remaining unbound population N, so that a plot of $\langle\lambda\rangle$ vs N should generate the same curve at all temperatures. Šrajer and Champion[35] demonstrated this result by relating the moments of the spectral line shape to the unliganded population during rebinding; we show here that the universal behavior reflects a simple general property of hole burning systems (subject to some limitations), and we apply this result to the data of Figure 1.

If a ligand-binding molecule such as Mb rebinds the ligand exponentially after photodissociation, the rate of rebinding

$$k(H,T) = A_0 \exp(-H/RT) \tag{3}$$

depends on the enthalpy barrier H of rebinding. If H varies between molecules, so that barriers of height between H and $H + \mathrm{d}H$ are found only with probability $g(\mathrm{H})\ \mathrm{d}H$ (with $\int_0^\infty g(H)\ \mathrm{d}H = 1$), then the fraction of molecules remaining unliganded a time t after photolysis is

$$N(t,T) = \int_0^\infty g(H)\ \mathrm{d}H \exp(-A_0 t \exp(-H/RT))$$

The mean (observed) value of any quantity $q(H)$ associated with these substates is

$$Q(t,T) = \int_0^\infty g(H)\ q(H)\ \mathrm{d}H \exp(-A_0 t \exp(-H/RT))$$

These relations can be rewritten as

$$N(t,T) = \int_0^\infty g(H)\ \mathrm{d}H\ \Theta(H/RT, A_0 t)$$

$$Q(t,T) = \int_0^\infty g(H)\ \mathrm{d}H\ q(H)\ \Theta(H/RT, A_0 t)$$

where

$$\Theta(H/RT, A_0 t) = \exp(-A_0 t \exp(-H/RT))$$

is known as the characteristic isothermal annealing function for first-order processes.[36] If $g(H)$ is much broader than RT, then $\Theta(H/RT, A_0 t)$ may be adequately approximated by a step function

$$\Theta(H/RT, A_0 t) \approx 0 \qquad (H < H_0) \tag{4}$$

$$\Theta(H/RT, A_0 t) \approx 1 \qquad (H > H_0)$$

where $H_0 \equiv RT \log(A_0 t)$. The integrals then simplify to

$$N(t,T) \approx \int_{H_0}^\infty g(H)\ \mathrm{d}H = N(H_0)$$

$$Q(t,T) \approx \int_{H_0}^\infty g(H)\ q(H)\ \mathrm{d}H = Q(H_0)$$

Since $N(H_0)$ and $Q(H_0)$ are functions only of H_0, Q can be described as $Q(N)$, a function only of N (although this function need not be single-valued). Thus a plot of Q vs N during rebinding generates the same curve at all temperatures. This result is subject to the conditions that (1) rebinding of each substate obey an exponential law (i.e., there are no relaxations or additional unliganded states) and (2) the width of $g(H)$ (and of the product $g(H)\ q(H)$) greatly exceed RT; it can then serve as a test for hole burning.

Figure 3 shows the ratio of the "global" SVD amplitudes $V_2(t,T)/V_1(t,T)$ plotted as a function of $N(t,T)$. (These global amplitudes, discussed in the next section, are obtained from SVD of the entire data set, rather than from SVD of data at individual temperatures. The method of temperature correction of these amplitudes, and the determination of $N(t,T)$, are described in detail below.) The quantity $V_2(t,T)/V_1(t,T)$, which describes the wavelength shift of the photoproduct spectrum of the remaining unliganded population, is an averaged property of the surviving substates and therefore serves as $Q(t,T)$. In the language of the above discussion, Figure 3 shows $Q(t,T)$ plotted as a function of $N(t,T)$ for a range of temperatures. The data at all T fall close to a single curve, implying $Q \approx Q(N)$ as expected for kinetic hole burning. Significant departure from this universal curve occurs only for $T \sim 300$ K and $N < 0.3$ and, as we discuss below, reflects the occupation of an additional state at higher T. The detailed analysis below confirms that the width of $g(H)$ ($\Delta H \sim 6$ kJ/mol) for MbCO in trehalose is sufficiently large compared to RT ($\approx$1.7 at 200 K) that the approximation in eq 4 is valid for this system.

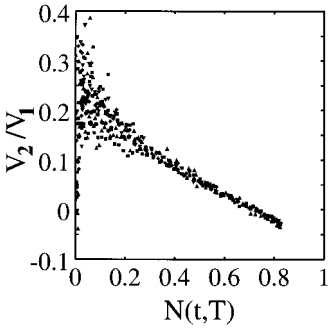

Figure 3. $V_2(t,T)/V_1(t,T)$ vs $N(t,T)$, showing "universal" curve for $T = 297-116$ K. Plotting the ratio V_2/V_1 instead of simply V_2 eliminates the factor $\beta_1(T)$ used in the temperature correction of both V_1 and V_2.

Global Data Analysis. We now turn to the quantitative analysis and fitting of the entire set of temperature-dependent data. Before comparing spectra collected at different temperatures, we first must account for the temperature dependence of the equilibrium MbCO and Mb Soret spectra, which produces differences in the amplitude, frequency, and shape of the Mb−MbCO difference spectra.[37] Small differences in the shape of $u_1(\lambda,T)$ and large differences in the shape of $u_2(\lambda,T)$ at different T are apparent in Figure 1a. The significant temperature dependence in the overall amplitude of the difference spectra is not evident in the $u_i(\lambda,T)$ because each basis spectrum is normalized to $|u_i|^2 = 1$.

To estimate the temperature-induced variation in the amplitude of the Mb−MbCO difference spectrum under the conditions of our experiments, we measured equilibrium spectra of Mb and MbCO (in trehalose) at temperatures between 300 and 100 K (Figure 4a,b) and synthesized from these data the Mb−MbCO difference spectra $B(\lambda,T)$ shown in Figure 4c. The largest effects of decreasing temperature are a sharpening of the MbCO Soret spectrum and an increase of its area. Both changes increase the amplitude of the Mb−MbCO spectrum. These effects (and other more subtle temperature effects) must be evaluated and corrected before the full set of spectra can be interpreted. We anticipate that, because the photoproduct Mb spectra are red-shifted (by 2−3 nm) with respect to the equilibrium Mb spectra, the MbCO and Mb Soret peaks may be nearer in wavelength for the reference spectra than for the photoproduct. Temperature-dependent changes in band shape may therefore have a greater effect on the amplitudes of the equilibrium spectra than on the photoproduct spectra. For this reason, in the fits to $N(t,T)$ described below, we first estimate the temperature-dependent change in extinction from the amplitude changes observed for the equilibrium spectra. We then permit this estimate to be refined in the course of further fits. Other temperature effects on the spectra include shifts in the peak positions for both the deoxy and CO absorption bands and changes in the shape of the Mb spectrum. These small effects are considered in our analysis of the time-dependent spectral shifts.

For data analysis and fitting it is convenient to represent all data in terms of a single set of temperature-independent spectra $\mathbf{U}(\lambda)$. We generated such a set by performing a "global" SVD of all time and temperature data together. In this procedure the data matrices for each T are interpolated onto a common wavelength and time grid and then appended along the time

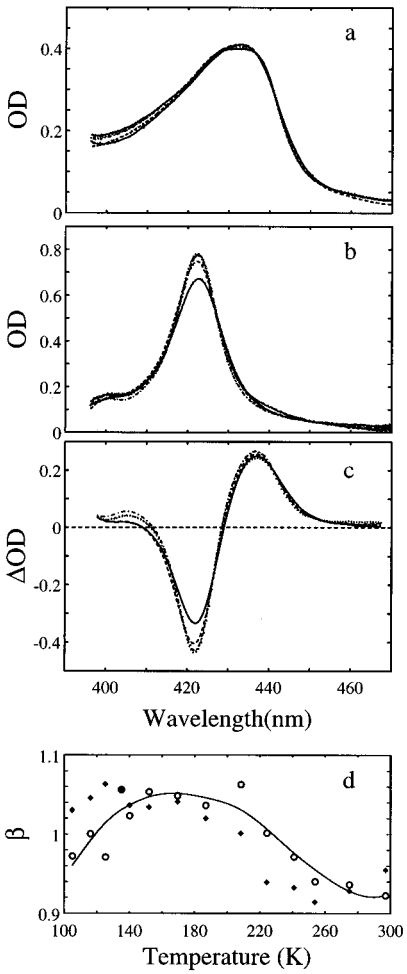

Figure 4. Equilibrium spectra for (a) deoxyMb and (b) MbCO in trehalose at $T = 302$, 241, 183, 144, and 115 K. As T decreases, the absorption peak for MbCO sharpens, while the deoxyMb peak flattens. (c) Difference spectra $B(\lambda,T)$ synthesized from above (unshifted) spectra. (d) Temperature correction $\beta(T)$ for the amplitude $V_1(t,T)$ of the first spectral component: (open circle) projection ($\propto\beta_1(T)$) of the difference spectra onto $U_1(\lambda)$; (solid curve) projection of difference spectra, smoothed with respect to temperature; (solid diamond) final corrections ($\propto\beta_1'(T)$) obtained from fit.

axis, forming a global data matrix $\mathbf{A}(\lambda,t,T)$. The SVD of this matrix,

$$\mathbf{A}(\lambda,t,T) = \mathbf{V}(t,T)\mathbf{S}\mathbf{U}(\lambda)^{\mathrm{T}}$$

shown in Figure 5, shows it to contain four significant spectral components $U_i(\lambda)$ with time-dependent amplitudes $V_i(t,T)$ that vary systematically with temperature.

The individual SVD analyses (Figure 1) revealed only two or three significant components in the data at each temperature. The additional components appearing in the global SVD arise from the temperature dependence of the underlying spectra. Since the average difference spectrum at each temperature $u_1(\lambda,T)$ differs from the global (i.e. all T) average difference spectrum $U_1(\lambda)$, the global SVD generates additional spectral components as corrections to $U_1(\lambda)$. The time-dependent amplitudes associated with such corrections are proportional at each temperature to the number of unliganded hemes, i.e., proportional to $V_1(t,T)$. The presence of these contributions in addition to the other spectral and kinetic information in the higher SVD components produces systematic effects in the $V_i(t,T)$. Therefore, temperature dependence in the difference spectra mixes $V_1(t,T)$ with the higher components (additively) and produces dramatic temperature dependence in the amplitudes $V_i(t,T)$ (Figure 5f) that is not apparent in the individual data sets (Figure 1e).

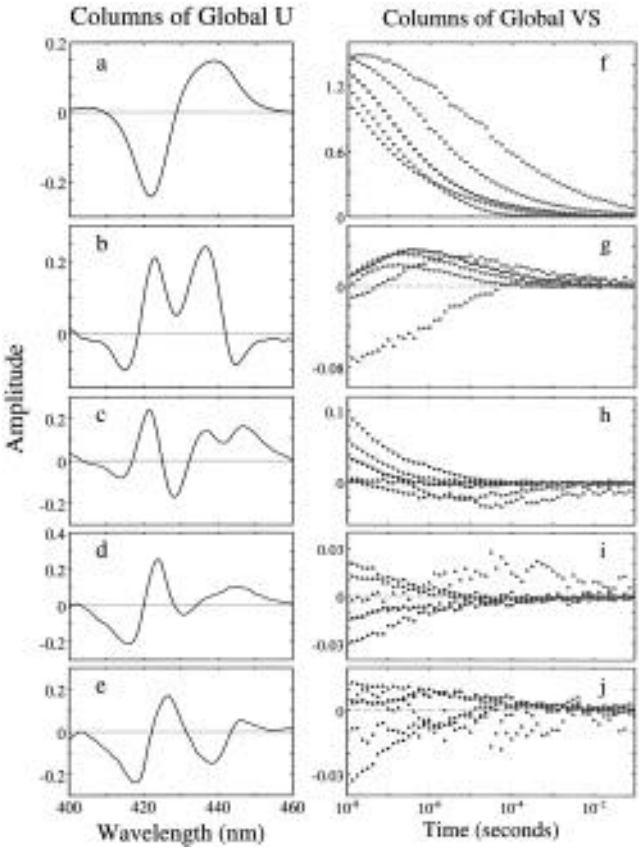

Figure 5. (a-e) Leading five spectral components $U_1(\lambda) - U_5(\lambda)$ obtained from global SVD of individual data sets, prior to Euler rotation (but after noise has been rotated to higher components). (f−j) Associated amplitudes $V_1(t,T)S_1 - V_5(t,T)S_5$ at $T = 297$ K (solid diamond), 241 K (solid down triangle), 208 K (solid circle), 152 K (solid box), and 105 K (solid up triangle).

Temperature Correction of V_1 and V_2. The temperature dependence of the amplitude of the Mb−MbCO difference spectrum (Figure 4c) appears in the initial amplitudes $V_1(t =$ 10 ns, $T)$, which grow by about 50% between 300 and 100 K (Figure 5f). While a portion of this increase reflects the temperature-dependent changes in the Mb−MbCO difference spectrum shown in Figure 4, a significant portion must result from real increases in the population $N(t,T)$ of hemes that are photodissociated at the end of the laser pulse. To account for the first of these effects, we write $V_1(t,T) = a(T)\ N(t,T)$, and anticipate that the coefficient $a(T)$ will exhibit significant temperature dependence. To obtain an initial estimate for $a(T)$, we represent the equilibrium spectra $B(\lambda,T)$, Figure 4c, in terms of the component spectra from the global SVD (through a least-squares fit):

$$B(\lambda,T) = \sum_i \beta_i(T)\ U_i(\lambda) \qquad (5)$$

We find a 15% increase in the amplitude $\beta_1(T)$ on cooling to cryogenic temperatures (Figure 4d). Therefore $V_1(t,T)$ must grow by approximately 15% at low T even if the number of unliganded hemes is the same in all experiments. In the fits described below, we use the values of $\beta_1(T)$ as a first-order correction, approximating $V_1(t,T)/\beta_1(T) \approx a_0 N(t,T)$ ($a_0 =$ constant) initially and refining this correction in subsequent fits.

Figure 6a shows the ligand rebinding data $N(t,T)$ after temperature correction. At $T \leq 220$ K, $N(t,T)$ exhibits smooth curvature consistent with a single (but nonexponential) ligand

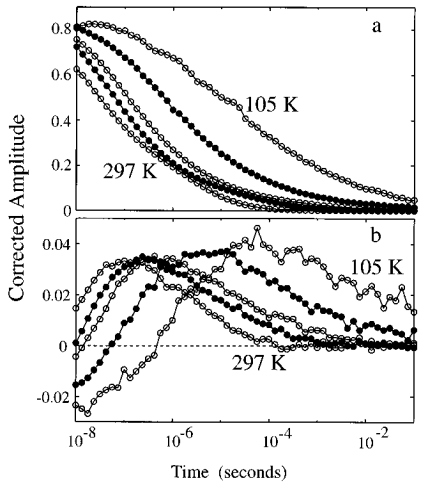

Figure 6. (a) $V_1(t,T)$ data (proportional to $N(t,T)$) after (final) temperature correction, at $T = 297$, 241, 208, 152, and 105 K. (b) Euler-rotated $V_2(t,T)$ after temperature correction with $\alpha_2(T)$, at the same temperatures.

binding process, while at $T \geq 240$ K a change in the curvature near $t \sim 10^{-6}-10^{-5}$ s clearly suggests an additional process. Curves at different temperatures do not cross. Because the initial level of photolysis $N(t=10\text{ ns},T)$ (i.e., 10 ns after the peak of the photolysis pulse) is approximately 30% larger at 100 K than at 300 K, we conclude that there exists a significant population of substates that rebind rapidly compared to the photolysis rate at high T but rebind more slowly near 100 K. To accommodate this result, we include in the fitting procedure the possibility that substates may rebind during the photolysis laser pulse. This allows a correct treatment at all temperatures of fast-binding substates that are only incompletely photolyzed at high temperatures.

We must also separate the effects of temperature from the kinetic effects in the time-dependent amplitudes $V_i(t,T)$ ($i = 2$, 3, 4). To do so requires that, at each temperature, we subtract from these amplitudes the $V_1(t,T)$ contribution that was introduced by the global SVD. This can largely be accomplished by the Euler rotation described by Ansari et al.[12] In this procedure, the second, third, and fourth spectral components are rotated $U_i(\lambda) \rightarrow U^{\text{rot}}{}_i(\lambda)$ ($i = 2-4$) until the new time-dependent amplitudes $V^{\text{rot}}{}_3(t,T)$ and $V^{\text{rot}}{}_4(t,T)$ are, at each temperature, as nearly as possible simply proportional to $V_1(t,T)$. The optimal rotation, shown in Figure 7, allows these two amplitudes to be expressed almost entirely as multiples of $V_1(t,T)$; the residuals contribute a maximum signal amplitude less than 20% as large as the amplitude contributed by the second SVD component. After rotation, these components primarily describe the temperature dependence of the difference spectra, while all significant time-dependent information is contained in the first and second SVD components. Therefore, in the following analysis we use $U_1(\lambda)$ and the rotated $U_2(\lambda)$ (and their associated amplitudes and singular values) as a compact representation of the data and we neglect the higher components.

Euler rotation does not necessarily remove all $V_1(t,T)$ admixture from $V_2(t,T)$. Temperature-induced spectral changes that resemble changes occurring kinetically during CO rebinding (i.e., wavelength shifts) will be represented by the same component spectrum $U_2(\lambda)$ and thus contribute some $V_1(t,T)$ amplitude to $V_2(t,T)$. We used the average difference spectrum at each temperature, $u_1(\lambda,T)$, to estimate this contribution. If all component species are represented to approximately the same extent in the average photoproduct at each temperature, the temperature dependence of the first spectral component $u_1(\lambda,T)$ of the individual (i.e., single T) data sets characterizes the average temperature dependence of the spectra of these species. Expressing $u_1(\lambda,T)$ in terms of the component spectra of the global SVD (in a least-squares fit)

$$u_1(\lambda,T) = \sum_i \alpha_i(T)\, U_i(\lambda)$$

shows that the amplitude $s_1(T)\, v_1(t,T)$ associated with $u_1(\lambda,T)$ accounts for a part $\alpha_2(T)\, s_1(T)\, v_1(t,T)$ in the total amplitude $S_2V_2(t,T)$ of the spectral component $U_2(\lambda)$. We approximate this contribution as $\alpha_2(T)S_1V_1(t,T)$ and subtract it from $S_2V_2(t,T)$:

$$S_2V_2(t,T) \rightarrow S_2V_2(t,T) - \alpha_2(T)S_1V_1(t,T)$$

or

$$V_2(t,T) \rightarrow V_2(t,T) - (S_1/S_2)\, \alpha_2(T)\, V_1(t,T) \qquad (6)$$

Finally, the same correction $\beta_1(T)$ applied to $V_1(t,T)$ (eq 5) is applied to $V_2(t,T)$. This is required because $U_2(\lambda)$ primarily represents a shift of the average difference spectrum, so a temperature-dependent increase in the magnitude of the difference spectrum will produce comparable changes in the magnitude of both $V_1(t,T)$ and $V_2(t,T)$. Together, these corrections remove most effects of spectral temperature dependence from $V_2(t,T)$. Our procedure for fitting $V_1(t,T)$ and $V_2(t,T)$ allows further refinement of the $\alpha_2(T)$ (see below). Figure 6b shows the final $V_2(t,T)$.

A Kinetic Hole Burning Model. Based on the initial evidence for inhomogeneous kinetics, we model the ligand binding kinetics with a distribution of conformational substates[2]

$$A_1 \leftarrow B_1 \leftrightarrow C_1$$

$$A_2 \leftarrow B_2 \leftrightarrow C_2$$

$$A_3 \leftarrow B_3 \leftrightarrow C_3$$

$$\ldots$$

$$A_m \leftarrow B_m \leftrightarrow C_m$$

In this description the conformational substates $i = 1 - m$ represent distinct, noninterconverting states of the myoglobin molecule. Within each substate i there are three states available to the CO ligand. Photodissociation of MbCO excites the CO from its bound state A_i to an unbound state B_i. From B_i the ligand may either rebind to A_i or else travel to a third state C_i within the protein. Passage between these states requires thermal activation over enthalpy barriers H_{BA}, H_{BC}, and H_{CB}, giving rise to Arrhenius rates

$$k_{BA} = A_{BA}(T/T_0)\exp(-H_{BA}/RT) \qquad (7)$$

$$k_{BC} = A_{BC}(T/T_0)\exp(-H_{BC}/RT)$$

$$k_{CB} = A_{CB}(T/T_0)\exp(-H_{CB}/RT)$$

where the prefactors A_{BA}, A_{BC}, and A_{CB} are constants, $R = 8.31$ J/(mol·K), and $T_0 = 180$ K. Following Austin et al.,[2] we assume that the rebinding barriers H_{BA} are different for different substates and that the probability of any molecule having a barrier height between H_{BA} and $H_{BA} + dH_{BA}$ is given by a probability distribution $g(H_{BA})\, dH_{BA}$. If interconversion between substates proceeds more slowly than ligand binding, the observed rebinding $B \rightarrow A$ for an ensemble of molecules is then multiexponential. This model assumes that conformational relaxation does not occur during rebinding. Instead, changes

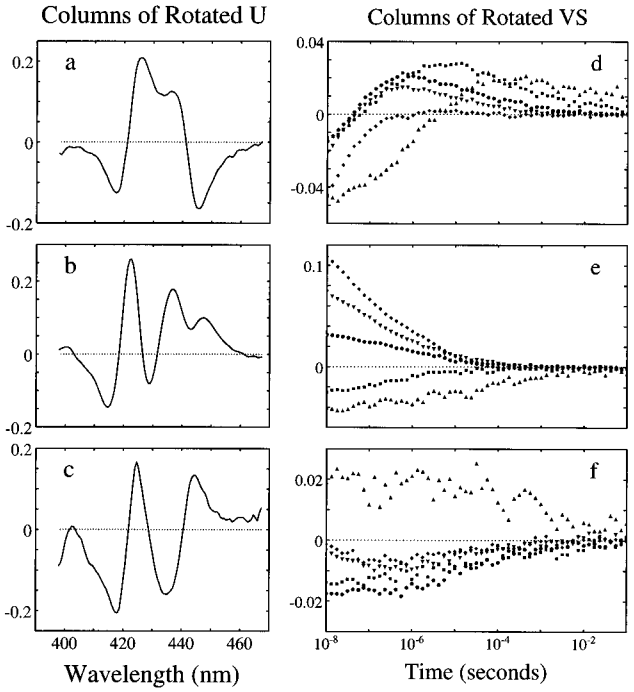

Figure 7. (a-c) Spectral components $U_2(\lambda) - U_4(\lambda)$ of the global SVD after Euler rotation. Data shown for temperatures $T = 297$, 241, 208, 152, and 105 K. (d−f) Amplitudes $V_2(t,T)S_2 - V_4(t,T)S_4$ after Euler rotation, at the same temperatures.

in the photoproduct spectrum during rebinding are interpreted as resulting from differences in the absorption spectra of molecules that rebind CO at different rates. In the following analysis we first demonstrate that $V_1(t,T)$ can be fit to this inhomogeneous model for $T \approx 100-300$ K, yielding the characteristic distribution $g(H_{BA})$. We then show that the concurrent spectral changes described by $V_2(t,T)$ are entirely consistent with hole burning from this distribution.

First SVD Component V_1. Rather than making an assumption about the functional form of $g(H_{BA})$, we seek a discrete approximation to $g(H_{BA})$ by fitting $V_1(t,T)$ to a histogram in H_{BA}. The range $H_{BA} = 0-28$ kJ/mol is divided into a uniform grid of enthalpies $H_{BA}{}^i = (i - 1) \times \delta H_{BA}$ (for $i = 1-m$) corresponding to m distinct protein substates, with each substate assigned a weight g_i (subject to $\sum_i g_i \delta H_{BA} = 1$) and a rate prefactor $A_{BA}{}^i$. We do not assume the $A_{BA}{}^i$ to be the same for all substates, but we do assume homogeneity in the outer rates, with the same barriers (H_{BC} and H_{CB}) and frequency factors (A_{BC} and A_{CB}) for all substates. The unliganded fraction $N_i(t,T)$ of hemes in each substate then decays biexponentially after photolysis according to the rate equations for the three-state kinetic scheme (eq 7), with the total fraction of unbound hemes given by

$$N(t,T) = \sum_i g_i N_i(t,T) \delta H_{BA}$$

We fit the temperature-corrected amplitude

$$V_1(t,T)/\beta_1(T) = a_0 N(t,T)$$

(a_0 = constant) to obtain the g_i, $A_{BA}{}^i$, A_{BC}, A_{CB}, H_{BC}, H_{CB}, and a_0. To obtain maximum fit quality without greatly increasing computation time, we fit for a reduced number m' of discrete values of $g(H_{BA})$ but interpolated $g(H_{BA})$ to higher density $m = 2m'$ (by cubic spline) in all kinetics calculations. Fits using $m' \leq 8$ reliably converged to a stable representation of $g(H_{BA})$ from any reasonable initial parameters (e.g., $g_0(H_{BA})$ = constant), while fits using $m' > 10$ generated a stable result if the initial parameters roughly approximated the $g(H_{BA})$ obtained from the $m' \leq 8$ fits. As shown below, the optimal number of substates for the fit was empirically determined to be $m = 32$ (or $m' = 16$), for which a reproducible $g(H_{BA})$ is readily obtained by gradually increasing the value of m in the fits.

As discussed above, the temperature corrections $\beta_1(T)$ only approximate the coefficients that relate $V_1(t,T)$ to $N(t,T)$. The best fit to the $V_1(t,T)$ was obtained by allowing the fit to refine these corrections. We fitted the $N(t,T)$ model to $V_1(t,T)/\beta_1(T)$ to determine $g(H_{BA})$ (and related parameters) and then used those results and the $\beta_1(T)$ as starting conditions in a new fit to $V_1(t,T)/\beta'_1(T)$ in which refined corrections $\beta'_1(T)$ were additional free parameters. The generated $\beta'_1(T)$ (Figure 4d) agree with the $\beta_1(T)$ to within the precision to which the $\beta_1(T)$ were calculated but give a generally smaller temperature correction to $V_1(t,T)$ (Figure 4d). Some of the temperature dependence in $V_1(t,T)$ is then apparently due to increased levels of photolysis at low T, implying that at high T some substates rebind during the 10 ns photolysis pulse. To allow for this possibility, the fitting routine calculates the rebinding rate $k_{BA}(T)$ for each substate, determines (by interpolation from tabulated values) the expected occupation of states A and B at $t = 10$ ns after photolysis by a Gaussian pulse, (i.e. photolysis rate $k_{AB}(t) = k^0{}_{AB} \exp(-t^2/2\tau^2)$, $k^0{}_{AB} \approx 1.7 \times 10^8$/s, $\tau \approx 4$ ns), and uses the result as the initial conditions for calculating the three-state kinetics of that substate.

Finally, the fits were optimized by varying the fit temperatures $\{T_j\}$ to minimize the sum-of-squares error in fitting $V_1(t,T)$. The resulting temperature adjustments $\langle \delta T^2 \rangle^{1/2} \approx 2.2$ K were generally consistent with the accuracy of the silicon diode thermometer (±1.5%). All fits were performed with a Marquardt−Levenberg algorithm that minimizes the sum-of-squares error $\sum_j (\delta V_1(j))^2$, with $\delta V_1(j)$ defined at each data point j by

$$\delta V_1(j) = V_1(j)_{data} - V_1(j)_{fit} + (0.01) \log(V_1(j)_{data}/V_1(j)_{fit})$$

This definition of the error emphasizes agreement on a linear N scale but does not allow small amounts of noise to interfere with fit quality on a logarithmic scale.

Figure 8 shows the results of the fit to $N(t,T)$ for $m = 32$. The agreement with the temperature-corrected data is excellent for $T = 105-254$ K and remains good to 297 K. Systematic deviation is apparent only at $T \approx 275-300$ K, near $t \sim 10^{-6}$ s. Figure 9a,c, shows the corresponding $g(H_{BA})$ and $A_{BA}(H_{BA})$. The enthalpy distribution is dominated by a single, nearly symmetric peak with $H_{BA}{}^{peak} \approx 6.5$ kJ/mol, $\langle H_{BA} \rangle \approx 7.8$ kJ/mol, and a full-width (half-maximum) of $\Delta H_{BA} \approx 6.2$ kJ/mol, but shows some additional structure at $H_{BA} > 20$ kJ/mol. $A_{BA}(H_{BA})$ shows a pronounced dependence on H_{BA}, varying by a factor ~100 through the main peak region of $g(H_{BA})$. The parameters for transitions between states B and C are found to be $\log(A_{BC}) \approx 12.9$ (+2.2, −0.68), $\log(A_{CB}) \approx 12.3$ (+1, −0.7), $H_{BC} \approx 37.5$ kJ/mol (±13.5), $H_{CB} \approx 34.2$ kJ/mol (±11). (The uncertainties represent the range of values for each parameter over which, when the remaining parameters are reoptimized, the fitting error increases by 50%.) The inset to Figure 8a shows the dependence of the sum of squares on m and demonstrates that $m = 32$ substates minimizes the fitting error.

The inhomogeneous frequency factor A_{BA} is important in obtaining a precise fit to $N(t,T)$. Figure 10 shows the fit to $N(t,T)$ if H_{BA} remains distributed but a *constant* frequency factor $A_{BA}{}^0$ is assumed to characterize all substates. The sum of squares increases by a factor ~7 in this fit because the calculated curves generally exhibit more temperature dependence than exists in the data (especially at $t \geq 10^{-5}$ s and $T \leq 220$ K).

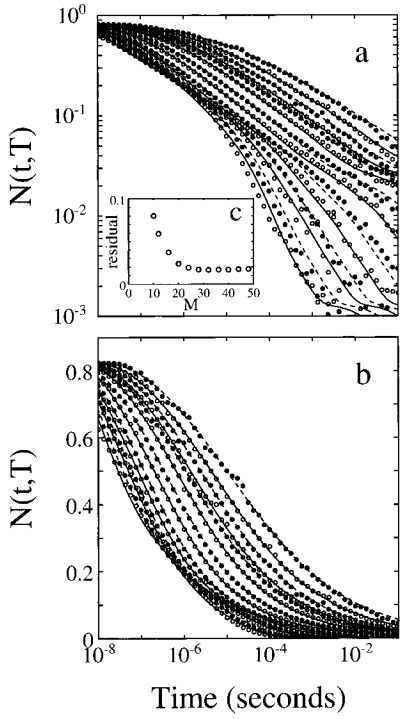

Figure 8. (a) Logarithmic plot of $N(t,T)$ (points) obtained from first SVD component, with fit (solid and broken lines) to $m = 32$ model. T = (from bottom) 297, 275, 254, 241, 224, 208, 187, 170, 152, 140, 135, 125, 116, and 105 K. Inset: Sum of squares fit error vs m (= number of bins in histogram used to define $g(H_{BA})$). (b) Semilogarithmic plot of $N(t,T)$ and fit to the $m = 32$ model. Same symbols as above.

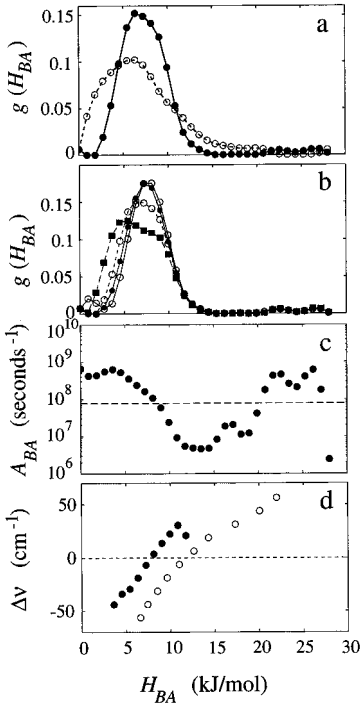

Figure 9. (a) $g(H_{BA})$ calculated from the final fit to $N(t,T)$ (solid circle), where A_{BA} is a function of H_{BA}; $g(H_{BA})$ obtained from a fit in which A_{BA} is required to be a constant, independent of H_{BA} (open circle). (b) $g(H_{BA})$ calculated from fits to $V_1(t,T)$ (which is proportional to $N(t,T)$) using different temperature corrections of $V_1(t,T)$: (open circle + solid line) no temperature correction to $V_1(t,T)$, i.e. assuming that $V_1(t,T) = a_0N(t,T)$; (solid circle + solid line) initial temperature correction $\beta_1(T)$ applied to $V_1(t,T)$; (open circles + broken line) final temperature correction $\beta'_1(T)$ applied to $V_1(t,T)$; (solid box + broken line) overcorrection, i.e. scaling $V_1(t,T)$ with the assumption that $N(t$=10 ns,$T) = 1.00$ for all T. (c) (solid circle) $A_{BA}(H_{BA})$ vs H_{BA} from final fit to $N(t,T)$; (broken line) A_{BA} obtained from fit in which A_{BA} is required to be a constant. (d) (solid circle) Soret frequency shift $\Delta\nu$ *vs.* geminate rebinding enthalpy H_{BA}, from "hole-burning" fit to amplitude $V_2(t,T)$ of second spectral component, using final $g(H_{BA})$ of Figure 9a; (open circle) $\Delta\nu$ of infrared band III *vs.* H_{BA}, obtained from hole-burning experiments at low T by Steinbach et al.[3]

Figure 9a shows the effect on $g(H_{BA})$. The assumption of uniform A_{BA} broadens $g(H_{BA})$ and spreads it asymmetrically toward higher enthalpies. The linear temperature dependence T/T_0 of the Arrhenius rate prefactor (eq 7) was established empirically: the residuals from a series of fits with rate prefactors proportional to $(T/T_0)^{\upsilon}$, with $0.33 \le \upsilon \le 2$, established that the fitting error was minimized for $\upsilon \approx 1$.

Figure 9b illustrates the effect of applying different temperature corrections to $V_1(t,T)$. The distributions $g(H_{BA})$ obtained from fits to $V_1(t,T)$ are shown for the four cases of (1) no correction, i.e., assume $a(T) = a_0$; (2) overcorrection, i.e., $V_1(t,T)$ scaled so that V_1 (t = 10 ns, T) = 1.00 for all T; (3) $V_1(t,T)$ corrected by the initial $\beta_1(T)$; and (4) $V_1(t,T)$ corrected by the refined $\beta_1'(T)$. While temperature correction of $V_1(t,T)$ is important, the figure shows that the features of the resulting $g(H_{BA})$ are not highly dependent on this correction. In addition to demonstrating that $V_1(t,T)$ can be fit by our kinetic model, these results show that the histogram method is a stable and simple technique for obtaining the distribution $g(H_{BA})$. The distributions are smooth and reproducible, and they require no assumptions about either the form of $g(H_{BA})$ or the enthalpy dependence of the rate prefactor $A_{BA}(H_{BA})$.

Second SVD Component V_2. We now analyze the second SVD component quantitatively. If substates having different rebinding enthalpies H_{BA} exhibit slightly different Mb−MbCO difference spectra $B(\lambda,H_{BA})$, then the average position and the detailed shape of the photoproduct spectrum will evolve in time as ligands rebind. Given the distribution $g(H_{BA})$, we can fit $V_2(t,T)$ to this hole-burning model if we represent the individual substate spectra as slightly shifted versions of the average spectrum $U_1(\lambda)$:

$$B(\lambda,H_{BA}) \propto U_1(\lambda) + x(H_{BA})U_2(\lambda)$$

Since $U_2(\lambda)$ approximates a wavelength derivative of $U_1(\lambda)$,

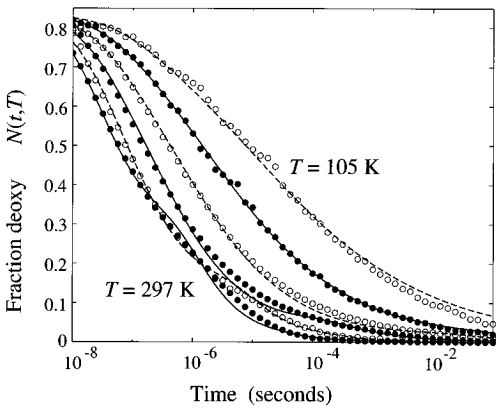

Figure 10. $N(t,T)$ vs t and T, data and fit with A_{BA} = constant. For clarity, only a subset of the data is shown. Temperatures are (from top) T = 105, 125, 152, 187, 241, and 297 K.

$x(H_{BA})$ is proportional to the Soret wavelength shift of each substate relative to the average spectrum. If the substate spectra are time-independent (i.e., there is no relaxation after photolysis), the time-dependent difference spectrum after photolysis can be written as a sum over the photoproduct distribution

$$\mathbf{A}(t,\lambda,T) \propto \sum_i g(H_{BA}{}^i)\, N_i(t,T)\, B(\lambda,H_{BA}{}^i)\delta H_{BA}$$

$$\propto \sum_i g(H_{BA}{}^i)\, N_i(t,T)\, U_1(\lambda)\delta H_{BA} + \sum_i g(H_{BA}{}^i)\, N_i(t,T)\, x(H_{BA}{}^i)\, U_2(\lambda)\delta H_{BA}$$

$$\propto N(t,T)\, U_1(\lambda) + [\sum_i g(H_{BA}{}^i)\, N_i(t,T)\, x(H_{BA}{}^i)\delta H_{BA}]\, U_2(\lambda)$$

Comparing this to the temperature-corrected SVD of the experimental data

$$\mathbf{A}(t,\lambda,T) \approx S_1(V_1(t,T)/\beta_1(T))\, U_1(\lambda) + S_2(V_2(t,T)/\beta_1(T))\, U_2(\lambda)$$

we see that $x(H_{BA})$ is obtained from a fit

$$S_2(V_2(t,T)/\beta_1(T)) = b_0 \sum_i g(H_{BA}{}^i)\, N_i(t,T)\, x(H_{BA}{}^i)\delta H_{BA}$$

Alternatively the constant b_0 and the $\beta_1(T)$ can be eliminated by fitting

$$V_2(t,T)/V_1(t,T) = (S_1/S_2)(\sum_i g(H_{BA}{}^i)\, N_i(t,T)\, x(H_{BA}{}^i)\, \delta H_{BA})/N(t,T)$$

We calculate $N_i(t,T)$ and $N(t,T)$ from the enthalpy distribution of Figure 8 and vary $x(H_{BA})$ to fit $V_2(t,T)/V_1(t,T)$. A fit with m substates has $m' = m/2$ free parameters x_1 ... $x_{M/2}$.

In fitting to $V_2(t,T)/V_1(t,T)$ we use a simple recursive scheme to refine the substate spectral shifts $x(H_{BA})$ and the temperature corrections $\alpha_2(T)$ (for correcting $V_2(t,T)$, eq 6). Because low enthalpy substates partially rebind during photolysis at $T \sim 300$ K but not at $T \sim 100$ K, the initial assumption that all substates are equally represented in the average photoproduct $u_1(\lambda,T)$ at any T introduces some error into the temperature corrections $\alpha_2(T)$ applied to $V_2(t,T)$. An error $\delta\alpha(T)$ adds an offset $\delta\alpha(T)S_1/S_2$ to the ratio $V_2(t,T)/V_1(t,T)$ (eq 6), causing a displacement of $V_2(t,T)/V_1(t,T)$ at each temperature relative to the curves calculated from the $x(H_{BA})$ fit. We adjust the coefficients $\alpha_2(T)$ by the amount of these shifts and recorrect $V_2(t,T)$ so that the V_2/V_1 data move closer to the fit curves. We then fit again to obtain a new $x(H_{BA})$ and use this to obtain a second set of corrections to the $\alpha_2(T)$, etc. This procedure readily converges to a stable set of $\alpha_2(T)$ and $x(H_{BA})$: each set of corrections to these parameters is about 10% as large as the previous set.

Figure 11 shows $V_2(t,T)/V_1(t,T)$ and the fit for the $g(H_{BA})$ of Figure 9. Agreement is excellent for $T \approx 100-260$ K and very good for $T \approx 280-300$ K. Figure 9d shows the spectral shift of the substates (relative to the average Mb photoproduct) obtained from the $V_2(t,T)$ fit: the low enthalpy, fast binding substates are seen to exhibit red-shifted spectra, as expected from our initial analysis, and the relationship between spectral shift and rebinding enthalpy is similar to that observed[3] in low-T hole-burning studies of infrared band III. Thus the inhomogeneous substate model precisely describes both the ligand rebinding data contained in $V_1(t,T)$ and the time-dependent photoproduct spectral changes characterized by $V_2(t,T)$.

Discussion

The time-resolved photolysis difference spectra collected on MbCO/trehalose for $T \approx 100-300$ K contain information about kinetic phenomena associated with ligand binding at these temperatures and about the intrinsic temperature dependence of the Mb and MbCO absorption spectra. Singular value decomposition (SVD) simplifies data analysis by representing the spectra in terms of a minimal set of independent spectral components $U_i(\lambda)$ and associated time- and temperature-dependent amplitudes $V_i(t,T)$. The temperature corrections applied to these amplitudes (as described in the preceding section) are elaborate but necessary. They move essentially all independent kinetic information regarding ligand rebinding and the accompanying spectral changes into the first two SVD components. These components can then be analyzed within a kinetic model. The third and higher SVD components then primarily describe the temperature dependence of the Mb and MbCO spectra, and therefore do not concern us here. Without these corrections it is not possible to make an accurate comparison of the fraction of ligands bound at different temperatures, to obtain the distribution of activation energies and rate prefactors, or to determine the kinetics of spectral changes.

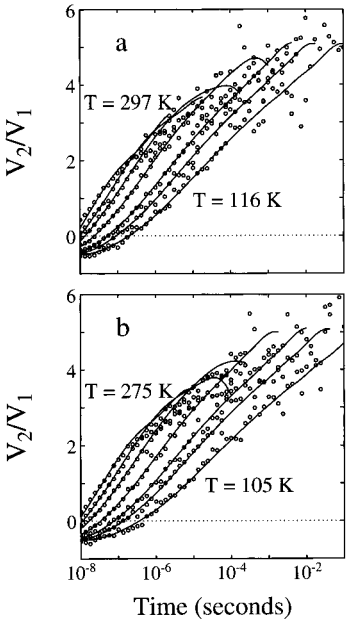

Figure 11. Data (open circles) and hole-burning model fit (solid curves) for temperature-corrected V_2/V_1 vs t, T. (a) T = 297, 254, 224, 187, 152, 135, and 116 K. (b) T = 275, 241, 208, 170, 140, 125, and 105 K.

The first significant amplitude $V_1(t,T)$ obtained from the SVD analysis is proportional at each temperature to the fraction $N(t,T)$ of molecules remaining unliganded a time t after photolysis. Unlike the complicated processes observed in other solvents, the behavior of $N(t,T)$ in trehalose is simple over the entire temperature range. For $T \approx 100-300$ K, $N(t,T)$ is consistent with geminate rebinding from an inhomogeneous system of conformational substates. This system can be characterized by the distribution $g(H_{BA})$ of activation enthalpies and the rate prefactors $A_{BA}(H_{BA})$. The second amplitude $V_2(t,T)$ in the SVD describes the progress of a time- and temperature-dependent wavelength shift of the Mb−MbCO difference spectrum as the CO rebinds. This spectral change could arise either from protein conformational changes during ligand rebinding or from differences in the absorption spectra of molecules that rebind at different rates (i.e., kinetic hole burning). Qualitative and quantitative evidence, including a "universal plot" (Figure 3), clearly indicates that at all temperatures studied the spectral shift results from kinetic hole burning rather than from conformational changes. We therefore fit $V_2(t,T)$ to a hole-burning model based on the enthalpy distribution $g(H_{BA})$ obtained from $V_1(t,T)$. This model assumes that a relationship exists between the rebinding enthalpy H_{BA} of a conformational state of the protein and the frequency shift $\delta\nu$ of the Soret difference spectrum of that substate (relative to the average difference spectrum). The

relationship $\delta\nu(H_{BA})$ obtained in the fit is nearly linear and resembles that observed for the porphyrin−iron charge transfer band III in the low-temperature hole-burning studies of Steinbach et al.[3] Together with the good quality of the fits to $V_1(t,T)$ and $V_2(t,T)$, this strongly implies that the kinetic model provides an accurate description of the rebinding process.

All spectral and kinetic information in the data can therefore be interpreted in terms of ligand rebinding by an inhomogeneous distribution of molecules with time-independent absorption spectra and strongly supports the conclusion that transitions between protein conformational substates occur on much longer time scales than ligand rebinding when the protein is embedded in trehalose. This appears to confirm the prediction of Ansari et al.,[9,12] who suggested that a sufficiently viscous solvent (such as a glass) might prevent both overall conformational relaxation and transitions between conformational substates following photolysis of myoglobin and therefore produce at all temperatures rebinding kinetics that closely resemble the multiexponential low T behavior. That high solvent viscosity can suppress all observable conformational changes at room temperature is a striking demonstration that the solvent plays an essential role in the structural dynamics of the protein. It shows that the conformational changes that control the observed kinetics must represent global changes of the configuration of the molecule, moving groups of atoms that may be in close contact with the solvent but far from the ligand binding site.

These results show that an important distinction must be made between solvent and protein effects on the rate of conformational changes. The conformational dynamics of myoglobin have been observed to slow dramatically when the protein is placed in a glycerol/water solvent and cooled to the vicinity of the solvent glass transition at $T_g \approx 180$ K. The viscosity dependence of the rate of conformational changes suggests that this slowing may result simply from rapid increase of the solvent viscosity near T_g, rather than from energy barriers intrinsic to the protein (although averaged over an equilibrium distribution of protein coordinates) that oppose conformational changes. Ansari et al.[12] noted that, given a Kramers-like viscosity dependence of the rate of conformational changes (eq 1) and the exponential growth[15] of the viscosity η of a glass-forming solvent near T_g,

$$\eta(T) \approx \eta_0 \exp((T_0/T)^2)$$

the rate κ^* of conformational changes would be expected to exhibit a highly non-Arrhenius slowing as $T \rightarrow T_g$. This rate

$$\kappa^*(T) \propto (\sigma + \eta(T))^{-1} \exp(-E_0/k_BT) \sim 1/\eta_0 \exp(-E_0/k_BT - (T_0/T)^2)$$

would likely be dominated by the strong temperature dependence of the viscosity, rather than by the activation energy E_0 associated with conformational changes. With Ansari et al.'s estimate $E_0 \approx 10$ kJ/mol in myoglobin and an estimate $T_0 \approx 1200$ K to describe the viscosity behavior of a 75% glycerol solution,[38] we expect that the temperature-dependent viscosity of a 75% glycerol solution would slow the rate of conformational relaxation in myoglobin by a factor $\sim 5 \times 10^8$ on cooling from 300 to 200 K, while the activation energy E_0 would slow this rate only by a factor ~10 over the same temperature range. Steinbach et al.,[3] who assumed that the rate κ^* of conformational relaxation in myoglobin intrinsically possesses a non-Arrhenius temperature dependence

$$\kappa^*(T) \sim \exp(-(T_1/T)^2)$$

found from fits to their ligand rebinding data that the characteristic value of T_1 in a 75% glycerol solvent was $T_1 \approx 1200$ K. This agrees perfectly with our estimate of T_0 for the glycerol/water solvent. That is, if protein conformational changes exhibit a Kramers-like viscosity dependence, the changing rate of conformational relaxation in myoglobin postulated by Steinbach et al. between 160 and 210 K is completely explained by the temperature dependence of the solvent viscosity. This is true nearly regardless of the activation energy scale E_0 associated with those conformational changes. The low T conformational dynamics of myoglobin may therefore reveal more about the low T viscosity of glycerol than about the energy barriers separating protein conformational substates.

A similar point was recently raised by Mayer.[39] Ansari et al.[17] and Iben et al.[16] noted that the interconversion between the A_0, A_1, and A_3 conformers of MbCO (observed by infrared spectroscopy) that occurs at high temperature is disrupted as the MbCO/solvent system is cooled below the solvent glass transition temperature T_g, and the protein falls out of equilibrium. These authors described the protein as undergoing a glass transition "slaved" to that of the solvent. Mayer[39] observed that in slightly hydrated MbCO the conformers interconvert continuously over the temperature range 78−293 K, suggesting that no single transition is associated with the protein in the absence of solvent. Mayer therefore questioned the glass description: the freezing of conformer populations in solutions at low T may reflect the rigidity of the glassy solvent rather than the energy scale of conformational changes in the protein molecule itself. Mayer's observation that, in the near absence of solvent, conformational equilibration occurs on time scales $t \leq \sim 10^2$ s at $T = 78$ K implies that this energy scale is not larger than $E \sim RT \ln(At) \sim 15-18$ kJ/mol (assuming a rate prefactor $A \sim 10^8-10^{10}$ s^{-1}). This is in good agreement with the estimate $E \approx 10$ kJ/mol of Ansari et al.[9,12] for the energy barrier associated with conformational relaxation of Mb after photolysis. A similar argument may therefore apply to all observable conformational changes, including interconversion between substates or conformers and the conformational relaxation that follows photolysis: as anticipated by Ansari et al.,[9,12] the rate of conformational changes is constrained more by solvent viscosity than by energy barriers intrinsic to the protein.

Studying the geminate kinetics of MbCO in trehalose provides an opportunity to observe the enthalpy distribution $g(H_{BA})$ associated with the unrelaxed conformations of the protein at room temperature. While our data show little evidence for conformational relaxation during rebinding, relaxation at subnanosecond times could affect the observed $g(H_{BA})$, since several authors[3,6,12,40] have suggested that conformational relaxation after photolysis slows geminate rebinding of CO by raising the average enthalpy barrier $\langle H_{BA}\rangle$. An examination of geminate rates, however, indicates that the observed $g(H_{BA})$ is that of the unrelaxed protein. The average geminate rate calculated from $g(H_{BA})$ at 300 K,

$$\langle k_{BA}(300\text{ K})\rangle = \int_0^\infty g(H_{BA})\, dH_{BA}\, k_{BA}(H_{BA}, 300\text{ K}) \approx 5.1 \times 10^7\text{ s}^{-1}$$

is approximately 20 times greater than the rate $k_{BA} \approx 2.4 \times 10^6$ s^{-1} estimated by Ansari et al.[12] for binding to the unrelaxed protein in glycerol/buffer. If conformational relaxation does slow the rate of geminate rebinding, the much higher rate obtained from our $g(H_{BA})$ strongly suggests that this distribution is characteristic of a protein molecule less relaxed than that studied by Ansari et al. Ansari et al. noted that the Soret spectral shift that they observed in Mb at times $t > 10$ ns after photolysis

was only ~30 cm^{-1}, or ~20% of the total expected shift[35] (~140 cm^{-1}). These authors therefore concluded that they had resolved only the last phase of an extended conformational relaxation in Mb, so that their estimate for the unrelaxed k_{BA} was in fact a lower bound to the true geminate rate for the unrelaxed protein. This conclusion was supported by time-resolved optical studies of band III,[11] which showed that most of the Mb conformational relaxation in glycerol/buffer occurs within ~3 ns of photolysis, i.e., beyond the time resolution of Ansari et al. The rapid geminate rate calculated from the $g(H_{BA})$ in trehalose is therefore entirely consistent with what is known about the geminate rate of the unrelaxed Mb molecule. Furthermore, the mean geminate rate in trehalose is approximately 2500 times greater than the rate $\langle k_{BA} \rangle \approx 2 \times 10^4$ s^{-1} observed for the fully relaxed protein in aqueous solvents,[12] which strongly supports the hypothesis that conformational relaxation slows the rate of geminate rebinding.

Some conformational relaxation may occur during ligand rebinding in the glass. Small systematic deviations in the fit to the rebinding kinetics $N(t,T)$ at $T \geq 280$ K and $t \sim 10^{-6}-10^{-4}$ s (Figure 8) suggest that the three-state model does not completely account for the observed high-temperature behavior. There are alternatives to the three-state model, which includes two geminate states (one with the ligand in the heme pocket, and a second with the ligand elsewhere in the protein) but no conformational relaxation. One alternative model might include only a single geminate state but allow for a protein conformational relaxation that decreases the rate of geminate rebinding. Ligand rebinding kinetics alone do not provide sufficient information to distinguish between such models. For example, the multiple-well model of Austin et al.[2] and Beece et al.[5] and the relaxation model of Steinbach et al.[3] both fit the ligand rebinding kinetics of MbCO in glycerol/water. A simultaneous measurement of the kinetics of spectral changes is needed if the models are to be distinguished. This was accomplished by Ansari et al.[12]

Evidence of relaxation is not apparent either in the fits to the spectral changes $V_2(t,T)$ or in the second spectral component $U_2(\lambda)$, which at all temperatures studied resembles the hole-burning signature (Figure 2). We have carried out similar studies on horse myoglobin in trehalose, in which the deviation from a single geminate phase at room temperature is observed to be even larger. This deviation must indicate either an additional geminate state or protein relaxation. Again the spectral changes $U_2(\lambda)$ are characteristic of kinetic hole burning (Hagen, Hofrichter, and Eaton, unpublished results). If conformational relaxation does cause the disagreement in Figure 8 it is evidently of smaller amplitude and slower rate ($\kappa^* \sim 10^4-10^6$ s^{-1} at $T \sim 300$ K) than the relaxation observed on the picosecond−nanosecond time scale in glycerol/buffer solvents at similar T.[9,11,12] This would support the sequential picture of the protein relaxation as a "local" initial motion followed by subsequent "global" phases.[41] The initial motion, confined to the heme−iron system, may be only weakly affected by solvent viscosity, while the global phase presumably repositions numerous protein atoms in close contact with the solvent and yields the equilibrium Mb structure. In this interpretation, a highly viscous solvent (i.e., trehalose) may completely suppress the global relaxation on the time scale of rebinding, yet only delay the local process. The small misfit in Figure 8 may then reflect this local relaxation, slowed by a factor ~10^6 from the picosecond to the microsecond regime.

The possibility of conformational relaxation below T_g is an interesting one. Relaxation of a protein in a glass would require that the modified Kramers equation, eq 1, provide for a nonzero limiting rate of relaxation at infinite solvent viscosity, as in eq 2. Recent studies have indicated that protein relaxation may occur in glycerol/water glasses after extended illumination at temperatures below the solvent glass transition ($T_g \sim 180$ K), as evidenced by Raman data[32] and by the slowing of geminate rebinding[19] of MbCO under such conditions. The mechanism for this "light-induced relaxation" is not clear. It has been proposed that the relaxation is a barrier-crossing process facilitated by the electronically excited state of the heme after absorption of a photon.[19] However, the excited state lifetime measured at room temperature is only ~300 fs,[42] while the conformational relaxation rate at the nominal temperature $T <$ 160 K of the experiment is only $\kappa^* \sim 10^{-7}$ s^{-1}, as extrapolated from the estimate of Steinbach et al.[3] The probability of relaxation during the excited state lifetime would therefore be undetectably small unless both (1) the lifetime is greatly lengthened at low temperatures and (2) the conformational relaxation rate is drastically enhanced. Another possible origin for the relaxation is that the heme is heated vibrationally by photon energy that exceeds the amount needed for photodissociation. Molecular dynamics simulations indicate that excess vibrational energy in the heme is transferred to the global, low-frequency modes of the protein, resulting in a relatively uniform temperature rise.[43] In a glassy environment, however, these modes would presumably be absent, and heating of the protein would be complex and nonuniform. It may be possible to evaluate such a heating mechanism through dynamics simulations. Experiments on the wavelength dependence of "light-induced relaxation" could also be useful.

The slowing of rebinding after extended illumination in the glass at low temperatures may result from causes other than relaxation of the protein. It has been argued[44,45] that the phenomenon instead indicates pumping of the ligand to additional, slowly rebinding geminate states. That is, if there exists a long-lived geminate state (equivalent to the state C in our kinetic model) that is accessible only by passage of the ligand over a sizable barrier, the ligand would eventually become trapped in that state if the sample were photolyzed repeatedly at low temperature. Šrajer et al.[45] estimated that the rate for the transition B → C is quite small at low temperature, yielding only a small probability (~5×10^{-7} near 100 K) for a photolyzed CO molecule to move from state B to state C before returning to A. We note that, in a kinetic model like ours, the probability that the ligand will move to state C after photolysis increases with temperature: therefore, any local heating of the heme complex by absorbed photons during extended illumination will tend to enhance the degree of pumping.[46] Thus, the light-induced slowing of geminate rebinding cannot yet be interpreted as evidence for conformational relaxation of the protein in the glass. It could therefore be very important to search directly for relaxation by measuring the subnanosecond kinetics of the shift of the charge-transfer band III of photolyzed deoxymyoglobin in the trehalose glass.[11] In any event, protein relaxation in the glassy state, if it indeed occurs, is an interesting question that will require considerable further investigation.

We now consider the relation between the activation energy distribution $g(H_{BA})$ observed in trehalose and that previously observed in other solvents. We have noted that the average geminate rate calculated from $g(H_{BA})$ in trehalose, $\langle k_{BA}(300\ K) \rangle \approx 5.1 \times 10^7$ s^{-1}, is ~2500 times greater than the average rate observed for the fully relaxed protein in aqueous solvents.[12] This rate is also comparable to the unrelaxed geminate rate $\langle k_{BA}(300\ K) \rangle \approx 3.5 \times 10^7$ s^{-1} predicted from the $g(H_{BA})$ distribution of unrelaxed Mb in glycerol/water at low temperature.[3] Because there is no spectral evidence for relaxation in trehalose during

rebinding, and because the average geminate rate in trehalose is at least as great as the fastest rates observed under other experimental conditions, we conclude that the trehalose $g(H_{BA})$ characterizes a state of the protein that is no more relaxed than the state observed in other experiments, such as the low-temperature studies of Steinbach et al. However, this conclusion is subject to a caveat. Temperature-derivative spectroscopy[47] indicates that the three A-state conformers of Mb exhibit different distributions $g(H_{BA})$ in the rebinding of CO. If the relative populations of the A states vary under different solvent conditions, the average geminate rate may vary as well. Therefore, the trehalose sample may exhibit rapid rebinding not solely because the Mb in trehalose is completely unrelaxed, but because the sugar favors an A state characterized by an especially low rebinding enthalpy. We note that Austin et al.[2] observed a very different distribution in PVA from that in glycerol/water, and Šrajer et al.[45] found that the enthalpy distribution in water may be shifted by ~3 kJ/mol relative to glycerol/water.

Significant differences in the $g(H_{BA})$ distributions for trehalose and glycerol/water strongly suggest that solvent composition affects the *A*-state populations. Figure 12 shows $g(H_{BA})$ and $A_{BA}(H_{BA})$ for MbCO in glycerol/buffer, calculated by our histogram method from the single-wavelength geminate kinetics data of Steinbach et al.[3] at $T = 60-150$ K. The histogram result agrees closely with the distribution obtained by Steinbach et al., who calculated $g(H_{BA})$ by fitting the model of Young and Bowne[48] to the same data, and by a maximum entropy fit.[49] Evidently $g(H_{BA})$ peaks at a much lower enthalpy in trehalose ($H_{peak} \approx 6.5$ kJ/mol) than in glycerol/water ($H_{peak} \approx 9.7-10.5$ kJ/mol) and is more symmetrical (nearly a single Gaussian). In fact, the histogram fit reveals structure in the glycerol/water $g(H_{BA})$, possibly resulting from the three A states, that has previously been detected only in temperature-derivative spectroscopy (in which rebinding to the individual A states is observed by infrared spectroscopy).[47] Therefore we fit $g(H_{BA})$, for both glycerol/water and trehalose simultaneously, as a sum of three Gaussian enthalpy distributions representing the A states of Mb. We assume that these distributions $g_0(H_{BA})$, $g_1(H_{BA})$, and $g_3(H_{BA})$ share the same width σ and are centered at H_0, H_1, and H_3 respectively. The fit yields the H_i (for $i = 0, 1, 3$), σ, and the relative populations a_i^{treh} and a_i^{glyc} of the A states in trehalose and in glycerol/water:

$$g_{treh}(H) = a_0^{treh} g_0(H) + a_1^{treh} g_1(H) + a_3^{treh} g_3(H) \quad (8)$$

$$g_{glyc}(H) = a_0^{glyc} g_0(H) + a_1^{glyc} g_1(H) + a_3^{glyc} g_3(H)$$

Figure 12 shows that eq 8 provides a good fit to both distributions. H_1 and H_3 agree closely with those measured by Berendzen and Braunstein,[47] while H_0 differs by ~2.4 kJ/mol. It therefore appears that differences in the A-state populations can account for the difference between the trehalose and glycerol/water distributions; apparently the trehalose sugar favors the A_0 conformer of Mb, while glycerol/water favors A_1. Given the different enthalpy distributions in the two solvents, the fact that both predict nearly the same average geminate rate at 300 K is perhaps unexpected.

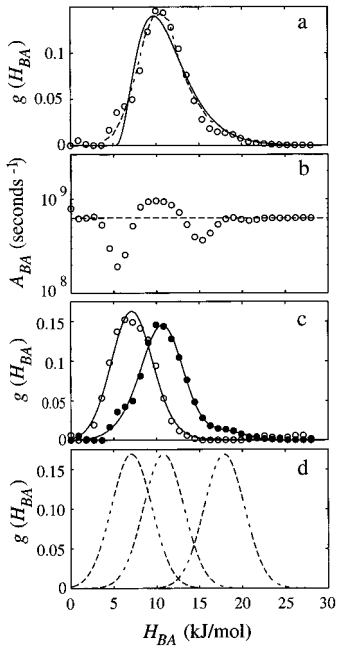

Figure 12. (a) Rebinding enthalpy distributions for MbCO in glycerol/buffer solvent at low *T*, calculated from fits to the photolysis data of Steinbach et al.:[3] (open circle) $g(H_{BA})$ calculated from histogram fit; (solid curve) $g(H_{BA})$ from Young and Bowne model[48] fit, from Steinbach et al.;[3] (broken line) $g(H_{BA})$ obtained from maximum entropy[49] fit. (b) Rate prefactor $A_{BA}(H_{BA})$ associated with $g(H_{BA})$: (open circle) $A_{BA}(H_{BA})$ calculated from histogram fit; (broken line) constant value $A_{BA} = 6.3 \times 10^8$ s^{-1} obtained from Young and Bowne model fit of Steinbach et al.[3] and assumed for maximum entropy fit.[49] (c) Rebinding enthalpy distributions for MbCO in glycerol/buffer solvent (closed circles) and for MbCO in trehalose (open circles). The distributions can be fit simultaneously (solid line) as the sum of three Gaussian functions of equal width σ, presumed to correspond to the $g(H)$ distributions of the three conformers A_0, A_1, and A_3 of MbCO (eq 8). (d) The Gaussian functions representing $g(H)$ for the three A states, obtained from the fit to the experimental $g(H)$ (eq 8). The functions are assumed to be unaffected by solvent composition; the fit allows only their relative weighting to vary for trehalose vs glycerol solvent. The fit gives the width $\sigma = 2.36$ kJ/mol, the center positions $H_0 = 7.1$ kJ/mol, $H_1 = 10.8$ kJ/mol, and $H_3 = 17.9$ kJ/mol of the three Gaussians, and the amplitudes $a_0^{treh} \approx 0.95$, $a_1^{treh} \approx 0.05$, $a_3^{treh} \approx 0$, $a_0^{glyc} \approx 0.10$, $a_1^{glyc} \approx 0.83$, and $a_3^{glyc} \approx 0.07$. Temperature-derivative spectroscopy[47] has given $H_0 \approx 9.5$ kJ/mol, $H_1 \approx 10.8$ kJ/mol, and $H_3 \approx 17.8$ kJ/mol.

Conclusions

We have shown that, in a solvent of sufficiently high viscosity, myoglobin at room temperature exhibits distributed, nonexponential ligand rebinding kinetics like those previously observed only at very low temperatures. We have also shown how a detailed analysis of these kinetics and the accompanying spectral changes can be performed from a set of photolysis difference spectra, despite the strong temperature dependence of the equilibrium absorption spectra of the protein. Our analysis separates these temperature-dependent effects and allows us to fit the kinetic and spectral data to a detailed model.

The suppression of both substate interconversion and conformational relaxation by the glassy solvent suggests that functionally significant conformational changes of the protein may correspond to large scale motions of the protein that displace solvent. This is consistent with the evidence[50] that the ligand affinities of heme proteins are strongly influenced by the displacement and orientation of the proximal histidine relative to the heme. Interconversion between functionally distinct substates would therefore require displacement of the entire F helix, which extends out to the protein−solvent interface. This is in contrast to isolated local motions such as side chain rotations, which may well exhibit a "glasslike" transition near 200 K in neutron-scattering studies[51] and molecular dynamics simulations[52] of lightly hydrated myoglobin. Our results, together with Mayer's studies[39] of conformational equilibration in myoglobin at low *T*, strongly imply that a glass

transition is not an intrinsic feature of the conformational kinetics of the protein.

Finally, it is interesting to note that in fluid solvents the earliest conformational changes observed in Mb at room temperature occur within a few picoseconds of photodissociation.[11] Because this time scale is comparable to the shear relaxation time of the aqueous solvent, the solvent response to these fast conformational changes is expected to resemble that of an elastic solid. Thus, at the fastest time scales, conformational changes in the protein should be very similar in water and in a glass.

Acknowledgment. We thank A. Szabo, P. Wolynes, and R. Zwanzig for helpful discussions, and C. Austen Angell for suggesting the use of trehalose as a glass. We also thank P. Steinbach, K. Chu, and H. Frauenfelder for kindly providing us with the raw kinetics data from ref 3, which we reanalyzed for our Figure 12.

References and Notes

(1) Greene, B. I.; Hochstrasser, R. M.; Weisman, R. B.; Eaton, W. A. *Proc. Natl. Acad. Sci. U.S.A.* **1978**, *75*, 5255. Chernoff, D. A.; Hochstrasser, R. M.; Steele, A. W. *Proc. Natl. Acad. Sci. U.S.A.* **1980**, *77*, 5606.

(2) Austin, R. H.; Beeson, K. W.; Eisenstein, L.; Frauenfelder, H; Gunsalus, I. C. *Biochemistry* **1975**, *14*, 5355.

(3) Steinbach, P. J.; Ansari, A.; Berendzen, J.; Braunstein, D.; Chu, K.; Cowen, B. R.; Ehrenstein, D.; Frauenfelder, H.; Johnson, J. B.; Lamb, D. C.; Luck, S.; Mourant, J. R.; Nienhaus, G. U.; Ormos, P.; Philipp, R.; Xie, Z.; Young, R. D. *Biochemistry* **1991**, *30*, 3988.

(4) Tian, W. D.; Sage, J. T.; Šrajer, V.; Champion, P. M. *Phys. Rev. Lett.* **1992**, *68*, 408.

(5) Beece, D.; Eisenstein, L.; Frauenfelder, H.; Good, D.; Marden, M. C.; Reinisch, L.; Reynolds, A. H.; Sorensen, L. B.; Yue, K. T. *Biochemistry* **1980**, *19*, 5147.

(6) Agmon, N.; Hopfield, J. J. *J. Chem. Phys.* **1983**, *79*, 2042.

(7) Kuriyan, J.; Wilz, S.; Karplus, M.; Petsko, G. A. *J. Mol. Biol.* **1986**, *192*, 133.

(8) Frauenfelder, H.; Sligar, S.; Wolynes, P. G. *Science* **1991**, *254*, 1598.

(9) Ansari, A.; Jones, C. M.; Henry, E. R.; Hofrichter, J.; Eaton, W. A. *Science* **1992**, *256*, 1796.

(10) Lambright, D. G.; Balasubramanian, S.; Boxer, S. G. *Chem. Phys.* **1991**, *158*, 249.

(11) (a) Lim, M.; Jackson, T. A.; Anfinrud, P. A. *Proc. Natl. Acad. Sci. U.S.A.* **1993**, *90*, 5801. (b) Jackson, T. A.; Lim, M.; Anfinrud, P. A. *Chem. Phys.* **1994**, *180*, 131.

(12) Ansari, A.; Jones, C. M.; Henry, E. R.; Hofrichter, J.; Eaton, W. A. *Biochemistry* **1994**, *33*, 5128.

(13) (a) Kramers, H. A. *Physica* **1940**, *7*, 284. (b) Hänggi, P.; Talkner, P.; Borkovec, M. *Rev. Mod. Phys.* **1990**, *62*, 251.

(14) (a) Jäckle, J. *Rep. Prog. Phys.* **1986**, *49*, 171. (b) Angell, C. A. *Science* **1995**, *267*, 1924.

(15) Bässler, H. *Phys. Rev. Lett.* **1987**, *58*, 767.

(16) Iben, I. E. T.; Braunstein, D.; Doster, W.; Frauenfelder, H.; Hong, M. K.; Johnson, J. B.; Luck, S.; Ormos, P.; Schulte, A.; Steinbach, P. J.; Xie, A. H.; Young, R. D. *Phys. Rev. Lett.* **1989**, *62*, 1916.

(17) Ansari, A.; Berendzen, J.; Braunstein, D.; Cowen, B. R.; Frauenfelder, H.; Hong, M. K.; Iben, I. E. T.; Johnson, J.; Ormos, P.; Sauke, T.; Scholl, R.; Schulte, A.; Steinbach, P.; Vittitow, J.; Young, R. D. *Biophys. Chem.* **1987**, *26*, 337.

(18) Frauenfelder, H.; Chu, K.; Nienhaus, G. U.; Young, R. D. In *Activated Barrier Crossing: Applications in Physics, Chemistry, and Biology*; Fleming, G. R., Hänggi, P., Eds.; World Scientific: River Edge, NJ, 1993; pp 120−138.

(19) Nienhaus, G. U.; Mourant, J. R.; Chu, K.; Frauenfelder, H. *Biochemistry* **1994**, *33*, 13413.

(20) Petrich, J. W.; Lambry, J.-C.; Kuczera, K.; Karplus, M.; Poyart, C.; Martin, J.-L. *Biochemistry* **1991**, *30*, 3975.

(21) Hagen, S. J.; Eaton, W. A. *J. Chem. Phys.* **1996**, *104*, 3395.

(22) Agmon, N.; Doster, W.; Post, F. *Biophys. J.* **1994**, *66*, 1612.

(23) Green, J. L; Angell, C. A. *J. Phys. Chem.* **1989**, *93*, 2880.

(24) Hagen, S. J.; Hofrichter, J.; Eaton, W. A. *Science* **1995**, *269*, 959.

(25) (a) Womersly, C. *Comp. Biochem. Physiol.* **1981**, *70B*, 669. (b) Crowe, J. H.; Crowe, L. M.; Carpenter, J. F.; Aurell Wistrom, C. *Biochem. J.* **1987**, *242*, 1.

(26) (a) Blakeley, D.; Tolliday, B.; Colaço, C.; Roser, B. *Lancet* **1990**, *336*, 854. (b) Colaço, C.; Sen, S.; Thangavelu, M.; Pinder, S.; Roser, B. *Bio/Technology* **1992**, *10*, 1007. (c) Roser, B. *BioPharm* **1991**, *4*, 47.

(27) Sikora, S.; Little, A. S.; Dewey, T. G. *Biochemistry* **1994**, *33*, 4454.

(28) Hagen, S. J.; Hofrichter, H. J.; Bunn, H. F.; Eaton, W. A. *Transfusion Clinique Biol.* **1995**, *6*, 423.

(29) Hofrichter, J.; Henry, E. R.; Ansari, A.; Jones, C. M.; Deutsch, R. M.; Sommer, J. *Methods Enzymol.* **1994**, *232*, 387.

(30) Henry, E. R.; Hofrichter, J. *Methods Enzymol.* **1992**, *210*, 129.

(31) Campbell, B. F.; Chance, M. R.; Friedman, J. M. *Science* **1987**, *238*, 373.

(32) Ahmed, A. M.; Campbell, B. F.; Caruso, D.; Chance, M. R.; Chavez, M. D.; Courtney, S. H.; Friedman, J. M.; Iben, I. E. T.; Ondrias, M. R.; Yang, M. *Chem. Phys.* **1991**, *158*, 329.

(33) Ormos, P.; Ansari, A.; Braunstein, D.; Cowen, B. R.; Frauenfelder, H.; Hong, M. K.; Iben, I. E. T.; Sauke, T. B.; Steinbach, P. J.; Young, R. D. *Biophys. J.* **1990**, *57*, 191.

(34) (a) Agmon, N. *Biochemistry* **1988**, *27*, 3507. (b) Agmon, N. *J. Phys. Chem.* **1990**, *94*, 2959.

(35) Šrajer, V.; Champion, P. M. *Biochemistry* **1991**, *30*, 7390.

(36) Primack, W. *Phys. Rev.* **1955**, *100*, 1677.

(37) Cupane, A.; Leone, M.; Vitrano, E.; Cordone, L. *Biopolymers* **1988**, *27*, 1977.

(38) The estimate $T_0 \approx 1200$ K for a glycerol/water mixture is based on (1) Bässler's finding[15] that $T_0 \approx 1295$ K for pure glycerol, (2) Bässler's finding that $T_0 = CT_g$, with $C = 6.0 \pm 0.5$ for glycerol-like solvents, (3) the fact [Rasmussen, D. H.; McKenzie, A. P *J. Phys. Chem.* **1971**, *75*, 967] that T_g in 75% glycerol is 15 K lower than in pure glycerol, giving T_0(75% glycerol) $\approx T_0$(pure glycerol) $- C(T_g$(pure glycerol) $- T_g$(75% glycerol)) $\approx 1205 \pm 8$ K.

(39) Mayer, E. *Biophys. J.* **1994**, *67*, 862.

(40) (a) Henry, E. R.; Hofrichter, J.; Sommer, J. H.; Eaton, W. A. In *Hemoglobins: Structure and Function*; Schnek, A., Paul, C., Eds.; Edition de l'Universite de Bruxelles: Brussels, 1983, pp 193−203. (b) Hofrichter, J.; Henry, E. R.; Sommer, J. H.; Deutsch, R.; Ikeda-Saito, M.; Yonetani, T.; Eaton, W. *Biochemistry* **1985**, *24*, 2667. (c) Scott, T. W.; Friedman, J. M. *J. Am. Chem. Soc.* **1984**, *106*, 5677.

(41) Ansari, A.; Berendzen, J.; Bowne, S. F.; Frauenfelder, H.; Iben, I. E. T.; Sauke, T. B.; Shyamsunder, E.; Young, R. D. *Proc. Natl. Acad. Sci. U.S.A.* **1985**, *82*, 5000.

(42) Petrich, J. W.; Poyart, C.; Martin, J. L. *Biochemistry* **1988**, *27*, 4049.

(43) Henry, E. R.; Eaton, W. A.; Hochstrasser, R. *Proc. Natl. Acad. Sci. U.S.A.* **1986**, *83*, 8982.

(44) Powers, L.; Chance, B.; Chance, M.; Campbell, B.; Friedman, J.; Khalid, S.; Kumar, C.; Naqui, A.; Reddy, K. S.; Zhou, Y. *Biochemistry* **1987**, *26*, 4785.

(45) Šrajer, V.; Reinisch, L.; Champion, P. M. *Biochemistry* **1991**, *30*, 4886.

(46) Of course, if it also enhances the rate of rebinding the net effect is unpredictable.

(47) Berendzen, J.; Braunstein, D. *Proc. Nat. Acad. Sci. U.S.A.* **1990**, *87*, 1.

(48) Young, R. D.; Bowne, S. F. *J. Chem. Phys.* **1984**, *81*, 3730.

(49) Steinbach, P. J.; Chu, K.; Frauenfelder, H.; Johnson, J. B.; Lamb, D. C.; Nienhaus, G. U.; Sauke, T. B.; Young, R. D. *Biophys. J.* **1992**, *61*, 235.

(50) (a) Friedman, J. M. *Science* **1985**, *228*, 1273. (b) Gelin, B. R.; Karplus, M. *Proc. Natl. Acad. Sci. U.S.A.* **1977**, *74*, 801.

(51) Doster, W.; Cusack, S.; Petry, W. *Nature* **1989**, *337*, 754.

(52) (a) Smith, J.; Kuczera, K.; Karplus, M. *Proc. Natl. Acad. Sci. U.S.A.* **1990**, *87*, 1601. (b) Loncharich, R. J.; Brooks, B. R. *J. Mol. Biol.* **1990**, *215*, 439.

JP960219T